



Compressive properties of porous Cu reinforced by inserting copper pillars or tubes

Jiangang Jia^{1,2} · Yongzhi Jing¹ · Diqiang Liu³ · Jiakang Ju¹ · Xiaoyu Wang¹ · Genshun Ji²

Accepted: 9 February 2021 / Published online: 18 February 2021

© The Author(s), under exclusive licence to Springer Science+Business Media, LLC part of Springer Nature 2021

Abstract

Open-cell metal foams suffer from severe deterioration in mechanical properties due to their enriched three-dimensional interconnected holes. In this paper, reinforcing copper pillar(s) or tube(s) are embedded into the foam matrix to form “composite” structure to enhance the open-cell copper foams. To do this, a simple positioning device is designed for preparation of the green porous copper aligned with directional through hole(s) based on a tapping method. Then the reinforcing pillar(s) or tube(s) are inserted into the hole(s) and sintered together. By this means, the mechanical properties of the copper foams are significantly improved. The energy absorption capacity of the composite foams has also been improved because of a higher and wider yield platform compared with the unreinforced copper foams.

Keywords Copper foam · Porous structure · Mechanical properties · Strengthening

1 Introduction

Metal foams have been of increasing interest since emergence due to their low density, impact energy absorption capacity, permeability, low thermal conductivity, and novel electrical and acoustic properties [1–4]. These properties mainly depend on the porosity (or relative density), base material, size and shape of the pores, open or closed cell structure, and pore distribution [2, 5]. The structures and mechanical properties of porous materials are affected by different preparation processes, which may fall into four broad classes [3, 6]: those in which gas is served as the blowing agent; those in which the foam is electro-deposited from an aqueous solution; those by infiltrating liquid metal into bed of granules followed by removing them; and those in which the foam is made by using various powder metallurgy (PM) methods.

Powder metallurgy strategy, normally involving co-pressing of a metal powder with a sacrificial space holder powder, can create open cell foams and has been successfully employed to produce various open- or partially open-pore metal foams [7–12]. Many kinds of materials like carbonate [8, 9], magnesium [10], sodium chloride [11] and even starch [12] can be used as spacers. As pore size and distributions are greatly influenced by spacers and fabrication processes, many research activities focus on optimization of some process parameters and the relationship between the foam mechanical performance and pore network features [13, 14]. In most cases, bigger pores result in higher strength and elastic modulus for the same porosity. Evidently, using coarser space holders leads to large pores and thicker cell walls. However, considerable difference in the particle size between metal powders and spacers causes some difficulties to control the homogeneity and uniformity of mixing, which in turn impair reproducibility for the pore structure of metal foams. Andrew. R. Kennedy’s group carried out a tapping-based method to intersperse metal powder with a spherical salt bead space holder [12, 15], highlighting the good reproducibility offered by the process which was achieved through precise control of the masses of powders and the compaction pressure. There are also studies on the preparation of copper foams using non-tapping method [16–19], which characterize by high flexibility in the ratio of spacer and copper powder material, but the connection of the cell unit may be

✉ Jiangang Jia
jjajg@lut.edu.cn

¹ School of Materials Science and Engineering, Lanzhou University of Technology, Lanzhou, China

² State Key Laboratory of Advanced Processing and Recycling of Non-Ferrous Metals, Lanzhou, China

³ Center of Materials Science and Optoelectronics Engineering, University of Chinese Academy of Sciences, Beijing, China

unsatisfactory. Other studies, like microporous copper foam prepared by the foaming method [20], and the nanoporous copper prepared by the hydrothermal synthesis process [21], are carried out mainly for functional applications.

Originating from the easily developed stress concentration surrounding the pores randomly distributed over the entire matrix, most metallic foams suffer from deteriorated mechanical properties. This drawback can be overcome by elongating the pores aligned of porous copper in the load bearing direction (frequently referred to as lotus-type structure) by employing unidirectional solidification method in pressurized inert atmosphere [1, 22–24]. A unidirectional longitudinal pore structure was also fabricated via explosive compaction of copper pipes [2], which exhibit excellent compressive properties with high energy absorption capability. Metal tubes (thin-walled shell structures) themselves, like metal foams, were widely used in area of shock resistance and energy absorption, and were attracted attention of many researchers [25–28]. However, reinforced metal foams with tubes or pillars has rarely been carried out. The aims of this study were to demonstrate a novel “composite” structure in which pillar(s) or tube(s) are embedded in Cu foam to improve the properties and reliabilities of the Cu foam based on a highly reproducible pore topology controlling process. The reinforced porous Cu structures have been characterized and their compressive mechanical properties are studied.

2 Experimental

2.1 Materials and preparation of green parts

Commercial purity Cu powder with a nominal size of 75 μm was used. Near-spherical NaCl beads were produced according to a method described in [11] (A. Jinnapat and A.R. Kennedy, 2011) and were sieved into size range of 1.0–1.5 mm. The morphology of the NaCl beads is shown in Fig. 2a. The two components were combined using a tapping-based method (illustrated in Fig. 1), similar to that reported in [11]. In the process, 8 g of NaCl beads were poured into the cavity of a 25 mm diameter die (with the bottom punch in place) and packing was enhanced by brief tapping using a Quantachrome AutotapTM machine, which employs a lifting and dropping action, tapping at roughly 4 Hz. 7 g of Cu powder was then placed on top of the beads bed, where after the top punch was inserted.

The process of the Cu powder into the bed of salt beads can be tracked by measuring the exposed height of the top punch as a function of the number of taps [15]. Measurement was made by interrupting tapping and (h_1-h_0) was recorded till it gets stable, at the time h_2 should be near equal to h_0 (see Fig. 1a). After interspersed by tapping, uniaxial die compaction was performed, at a pressure of 200 MPa, to

produce robust Cu–NaCl “composite” pellets. A typical “composite” pellet example is shown in Fig. 2b.

In order to insert the reinforcing pillar or tube into the copper matrix, samples with one or three unidirectional holes were made with the aid of a set of gaskets and locating pins. A schematic of the whole layered assembly and the gasket specifications are respectively shown in Fig. 1b and c. The NaCl was removed by immersion of the Cu–NaCl “composite” green body in warm water for around 3 h and subsequent drying at 80 °C for a minimum of 2 h. Afterwards, the locating pillar was recycled and replaced with the reinforcing copper pillar(s) (diameter of 3 mm) or tube(s) (out diameter of 3 mm and thickness of 0.25 mm) for further sintering.

2.2 Sintering

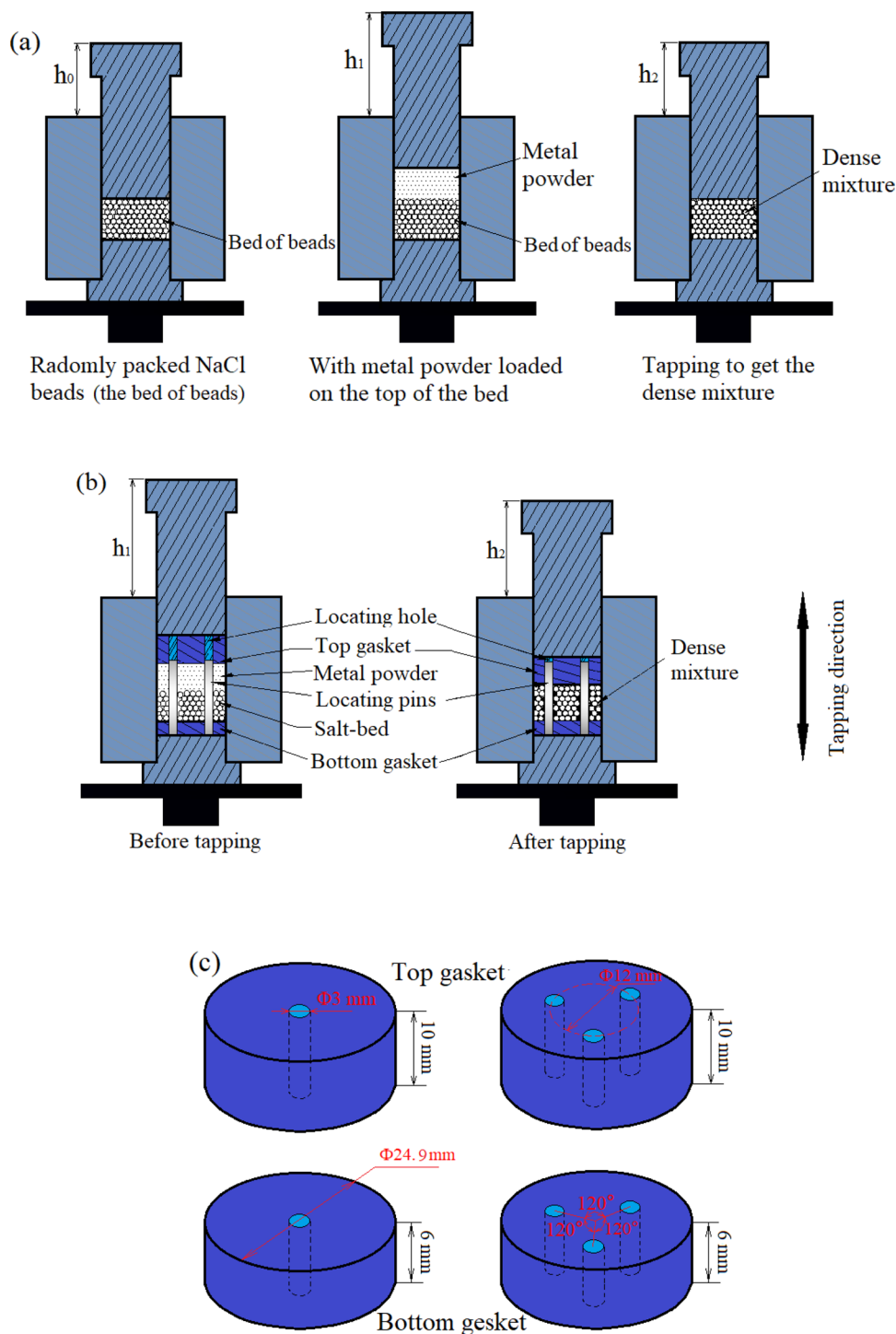
The green porous Cu samples were sintered in a tube furnace under an H_2 gas shield. Before heating, the furnace tube was evacuated using a vacuum pump and refilled with pure H_2 , cycling through this process for three times. With H_2 flowing through the tube at a rate of 120 ml min^{-1} , the temperature of the furnace was ramped up to 120 °C at a rate of 5 °C min^{-1} and held at this temperature for 30 min to remove any moisture. Thereafter the furnace was raised to 810 °C at a rate of 5 °C min^{-1} and held for 60 min. The as sintered samples are illustrated in Fig. 3. Samples with 0-, 1-, and 3-unidirectional holes in the first row of Fig. 3 are designated as S1, S2 and S3, respectively. The porous Cu samples reinforced with single pillar, 3 pillars, single tube and 3 tubes are referred as S4, S5, S6 and S7, respectively.

2.3 Characterization of porous copper parts

The densities of porous samples were measured from their dimensions and mass. Sintered structures were sectioned, and then were ground and polished by hand, without water, on metallographic preparation wheels for observations using optical microscopy (OM) and scanning electron microscopy (SEM). Compressive testing of porous structures was performed using an AGS-X-300KN Universal Testing machine, at a rate of 0.5 mm min^{-1} . Samples for the compressing test have a diameter of 24 mm and are ground to a height of 10 mm. Each testing condition was repeated on at least three samples, over which the compressive strengths were averaged.

In order to investigate the strengthening mechanisms under compressions, a number of samples reinforced with Cu pillar(s) or tube(s) were compressed to certain deformation stages, say at nominal strain of about 0.04, 0.2, 0.4 and 0.6, and then were sectioned through the mid plane of the reinforcing pillar(s) or tube(s) along the compressive direction to observe the deformation process. Since

Fig. 1 Schematic of the interspersed method, showing the powder layers and the distance measured to determine the height of the punch in the die and the gasket specifications



imaging the section structure requires destructive slicing of the samples, an individual sample needs to be used for each pre-designated strain. The strengths of 1-Cu pillar (tube) or 3-Cu pillars (tubes) were also tested. For testing the strength of 3-Cu pillars and/or 3-Cu tubes, the 3-Cu pillars or tubes were fixed with a piece of Cu foil on one side to maintain the relative poisoning as they were in the Cu foam sample.

3 Results

3.1 Porous structures and densities

Precise control of the shape, size and distribution of pores helps to reduce the wide scatter of physical and other characteristics of porous materials and components. Figure 2b demonstrates that the homogeneity of NaCl bead

spacer-copper powder blend within a part; Fig. 3 illustrates the homogeneity of porous structures from part to part. The photographic and SEM images, respectively shown in Fig. 4a and b, show that the pores remain the shape of the

salt beads (near spherical) after compaction and are connected by small windows. The connecting windows are formed due to incomplete filling of the cavities between the salt beads, i.e., the Cu powder particles cannot fit into the

Fig. 2 Photographic images of **a** NaCl beads: 1.0–1.5 mm and **b** Cu–NaCl “composite” pellet

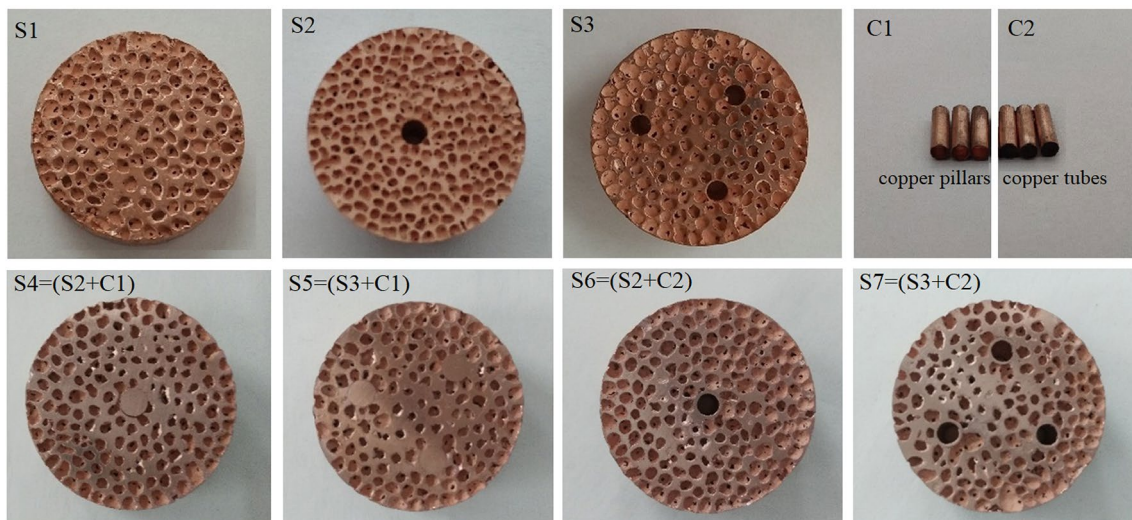
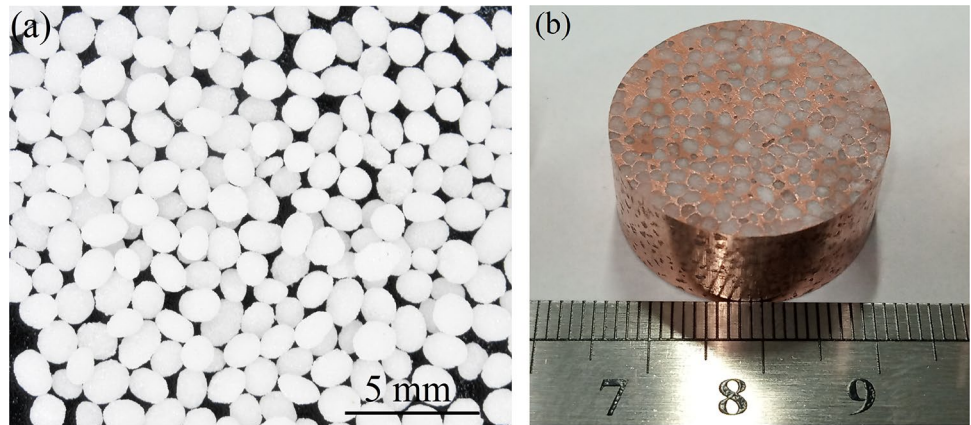
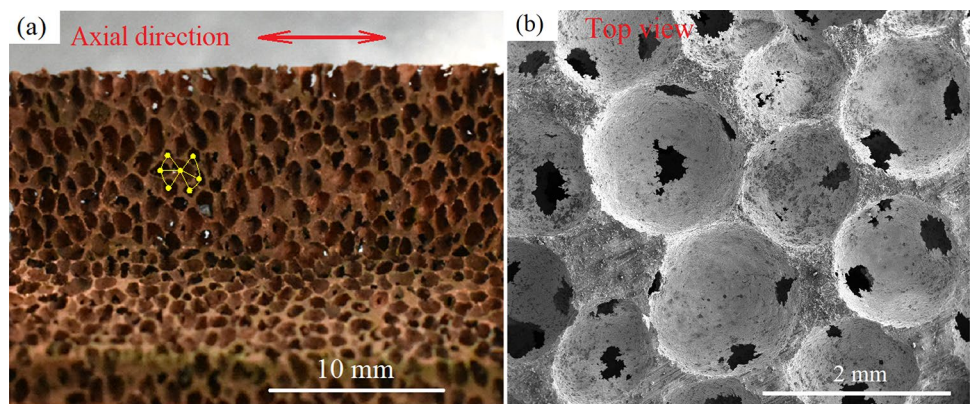


Fig. 3 Codes and images of the sintered porous Cu samples and the copper pillars and tubes

Fig. 4 Photographic (a) and SEM (b) image showing the cell structure and connectivity within the cell walls



small spaces at the contact points between neighboring salt spheres. The average number of the nearest neighbors for a particular cell (the coordination number) is around 6, which is in accordance with the number of the connecting windows in a cell (an average number of 3 windows in half a cell).

Densities of the Cu foam samples are listed in Table 1. We can see that the densities of S1, S2 and S3 are 1.31 g cm⁻³, 1.29 g cm⁻³ and 1.25 g cm⁻³, respectively. Obviously, processing unidirectional holes in the Cu foam results in higher porosity and lower density. Because the density of both C1 and C2 is higher than that of S1, incorporating C1 or C2 into S1 will increase the whole density of the foam structure. So, the densities of S4, S5, S6 and S7 are 1.45 g cm⁻³, 1.81 g cm⁻³, 1.40 g cm⁻³, and 1.52 g cm⁻³, respectively, each of which is above S1. Taking the density of the wall of Cu tube as 8.92 g cm⁻³ (the theoretical value), the calculated density of the C2 (Cu tube) is 2.72 g cm⁻³. The relative density and porosity of the samples are listed in Table 1.

3.2 Mechanical behaviors of the Cu foams

Typical compressive load–displacement curves for S4 (compared with S1 and S2), S5 (compared with S1 and S3), S6 (compared with S1 and S2) and S7 (compared with S1 and S3) are shown in Fig. 5a–d, respectively. Like other typical metal foams, S1 shows linear elasticity at low stresses followed by a long yield plateau, and terminate by a regime of densification in which the load (or stress) rises steeply. An increase in porosity (i.e. decrease in relative density) results in a decrease in the plateau load level and shortening of the densification displacement. So, S1 has higher compressive strength than S2 and S3.

The compressive response for S4 (Cu foam reinforced with 1-Cu pillar) is featured by a linear elasticity at low stresses, a slow strain hardening characteristic at the intermediate strain range follow by a short plateau and

a sharply risen slope at the large strain. For S5 (Cu foam reinforced with 3-Cu pillars), however, the load linearly increases with the displacement under 3 kN and continues to ramp up with a slightly decreased slope to maximum, and then the load drops rapidly by about 48% of the peak value before entering the densification stage. Clearly the compressive response for S5 does not show the characteristics of typical metal foams. Nevertheless, S6 (Cu foam reinforced with 1-Cu tube) and S7 (Cu foam reinforced with 3-Cu tubes) demonstrate similar load–displacement characteristics but improved strength compared with that of S1.

The mechanical properties of the Cu foams are list in Table 2, where σ_y represents the yield stress, ϵ_y the yielding strain, $\sigma_{pl}^{*,t}$ the plateau stress at the terminal point of the plateau, $\epsilon_{pl}^{*,t}$ the strain corresponding to $\sigma_{pl}^{*,t}$, σ_d the densification stress, ϵ_d the densification strain, and $\bar{\sigma}_{pl}^*$ the collapse stress (the average value of the plateau stress). The (σ_y, ϵ_y) is determined by the intersection of two tangents schematically depicted in Fig. 5a (see point A); the $(\sigma_{pl}^{*,t}, \epsilon_{pl}^{*,t})$ and (σ_d, ϵ_d) are corresponding to points B and C respectively, as depicted in Fig. 5b. From Table 2 we can see that the σ_y of S1 is 3.03 MPa, whereas the yielding stress of the Cu foams with 1 or 3 through unidirectional holes significantly decreased. The σ_y of S2 and S3 are 1.20 and 0.96 MPa, respectively. After inserting with Cu pillar(s), however, the foam structure is greatly strengthened. The σ_y of S4 is 6.84 MPa, which is 125.74% higher than that of S1. The $\sigma_{pl}^{*,t}$ and $\bar{\sigma}_{pl}^*$ of S4 are also much higher than those of S1, but the $\epsilon_{pl}^{*,t}$ for S1 and S4 are comparable. S5 shows a σ_y value of 18.91 MPa, which is the highest of all the foam samples. The σ_y of S6 and S7 are 4.24 and 4.75 MPa, which is 39.93 and 56.77% higher than that of S1, respectively. S6 and S7 are comparable in $\sigma_{pl}^{*,t}$ and $\bar{\sigma}_{pl}^*$, and both are higher than S1. Although different Cu foam samples have different strengths, the variation of σ_d values are less significant as that of σ_y , $\sigma_{pl}^{*,t}$ and $\bar{\sigma}_{pl}^*$ values because σ_d features deformation resistance of the dense state of a compressed foam. Clearly, the strengths of the Cu foams are significantly increased by inserting the Cu pillar or pillars. But considering the increase in density and, that the deformation of S5 has lost the feature of typical metal foam, the 3-Cu pillars reinforcing Cu foam may not be an effective way. Whereas Cu foams reinforced with Cu tube or tubes has moderate increase in density and distinct improvement of strength, as evidenced in Table 2.

Figure 6a shows the compressive load–displacement curves for the 1-Cu pillar and 3-Cu pillars. Simillar as the curves of a metal foam, the elastic loading region of the 1-Cu pillar or 3-Cu pillars is followed by a plateau, which might correspond to the stress deflection by plastic

Table 1 Densities of the Cu foam samples and the reinforcing Cu pillar and tube

Code of the sample	Density/g cm ⁻³	Relative density	Porosity/%
S1	1.31	0.1469	85.31
S2	1.29	0.1446	85.54
S3	1.25	0.1401	85.99
S4	1.45	0.1618	83.82
S5	1.81	0.2020	79.80
S6	1.40	0.1562	84.38
S7	1.52	0.1696	83.04
C1	8.92	1	0
C2	2.72	0.3056	69.44

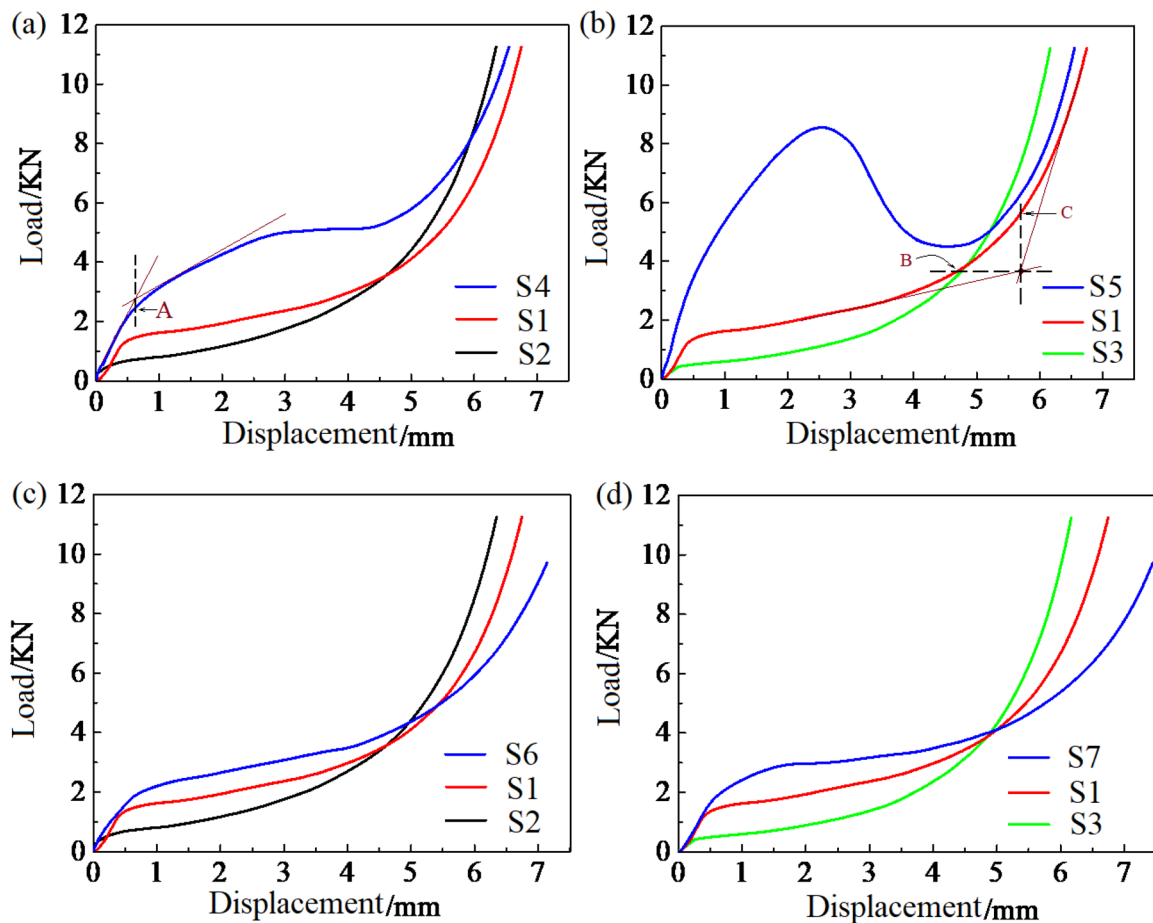


Fig. 5 Typical compressive load–displacement curves for the Cu foam samples: **a** S4 compared with S1 and S2, **b** S5 compared with S1 and S3, **c** S6 compared with S1 and S2 and **d** S7 compared with S1 and S3

Table 2 Mechanical properties of the Cu foam samples

Notes	σ_y /MPa	ϵ_y	$\sigma_{pl}^{*,t}$ /MPa	$\epsilon_{pl}^{*,t}$	σ_d /MPa	ϵ_d /MPa	$\overline{\sigma_{pl}^*}$ /MPa
S1	2.99 ± 0.23	0.05 ± 0.02	7.14 ± 0.67	0.45 ± 0.02	11.16 ± 0.53	0.55 ± 0.02	5.07 ± 0.45
S2	1.13 ± 0.09	0.02 ± 0.004	4.25 ± 0.21	0.32 ± 0.03	10.60 ± 0.49	0.51 ± 0.04	2.69 ± 0.15
S3	0.96 ± 0.06	0.01 ± 0.002	3.54 ± 0.38	0.33 ± 0.02	9.02 ± 0.14	0.50 ± 0.01	2.25 ± 0.22
S4	5.94 ± 0.27	0.08 ± 0.04	11.45 ± 1.98	0.46 ± 0.05	13.67 ± 2.54	0.54 ± 0.03	8.70 ± 1.26
S5	18.91 ± 0.71	0.25 ± 0.06	–	–	–	–	–
S6	3.91 ± 0.58	0.06 ± 0.02	7.93 ± 1.44	0.45 ± 0.06	9.68 ± 1.15	0.53 ± 0.05	5.92 ± 1.01
S7	4.58 ± 0.67	0.07 ± 0.03	8.44 ± 0.91	0.45 ± 0.04	9.94 ± 1.13	0.53 ± 0.02	6.51 ± 0.79

buckling (or folding) of the Cu pillar(s), as shown in Fig. 7a. The third stage is also an increase in the slope, corresponding to final densification. Apparently, the load levels for the plateau of the 3-Cu pillars are higher than the load levels for the plateau of the 1-Cu pillar.

The mechanical response of the Cu tube(s) is quite different from that of the Cu and/or the metal foams. According to Fig. 6b, the load–displacement curve for the 1-Cu tube or 3-Cu tubes can also be divided into 3 steps: (1) Elastic stage, the Cu tube has elastic deformation (stress and

strain are roughly linearly related) till the compression load reaches the greatest value when the material starts yielding; (2) Yielding plateau stage, as shown in Fig. 7b and c, the Cu tube(s) wrinkles and folds regularly and the load–displacement exhibits a region marked by several rises and falls, and at the same time, it can be regarded as a constant value and a plateau is formed; (3) Compact stage, wrinkles and folds are transmitted to the lowest part of the structure, like the final densification stage of the metal foams, the load–displacement curve is increasing steeply.

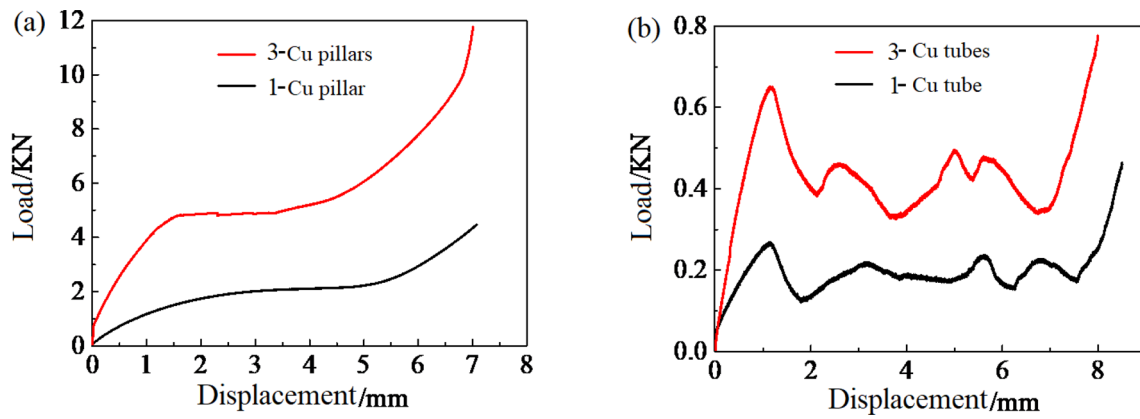


Fig. 6 Typical compressive load–displacement curves for the Cu pillar(s) (a) and tube(s) (b)

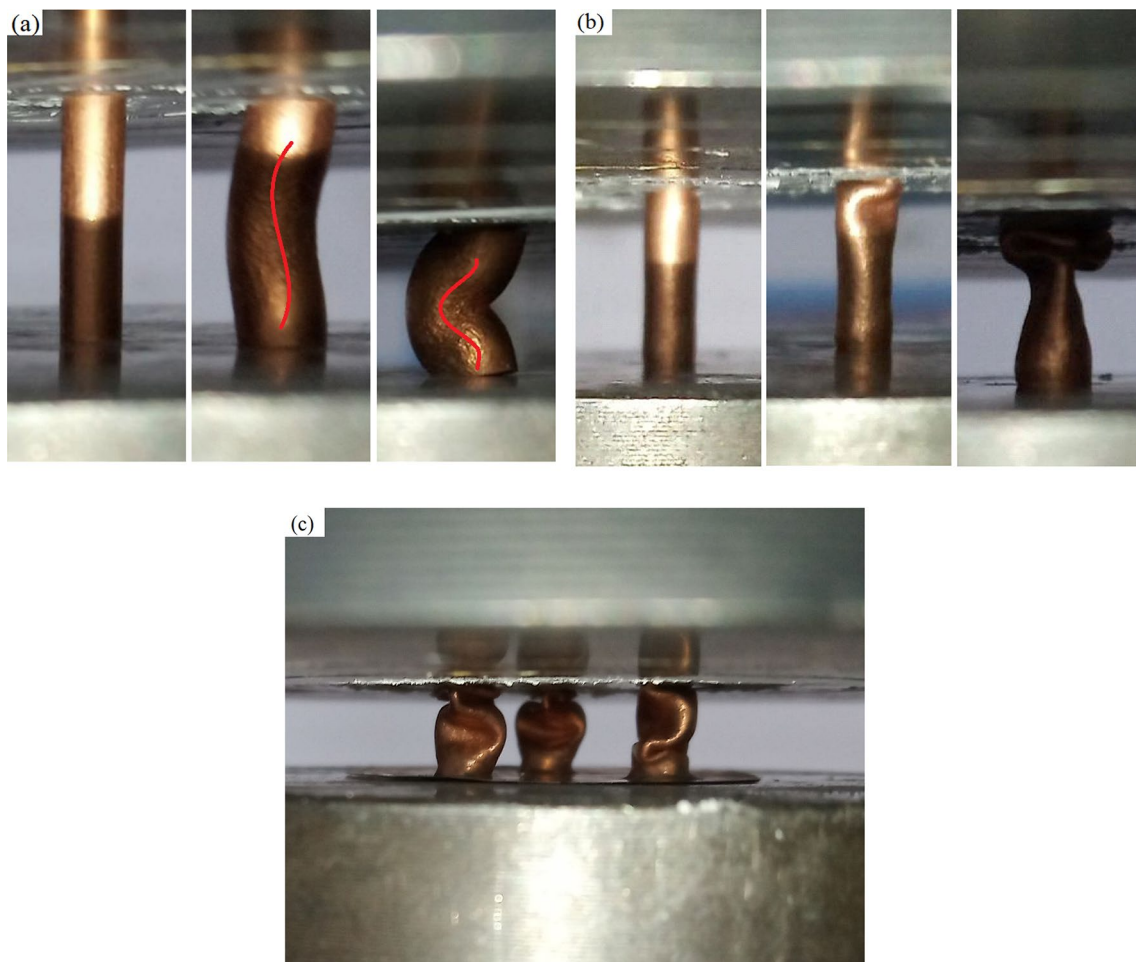


Fig. 7 Deformation morphology of the Cu pillar at the strain rate of 0.04, 0.2 and 0.4 (a), Cu tube at the strain rate of 0.04, 0.2 and 0.4 (b) and the 3-Cu tubes at strain rate of 0.6 (c)

4 Discussion

Porous copper produced by replication of the beads bed based on tapping method has the advantage of precise controlling over size and morphology of the pores. Owing to the use of a narrow size range of near-spherical NaCl beads, the packing fraction of the beads and the Cu accommodated in the network of the beads remains unchanged both within and from part to part, leading to Cu foams with uniform pore sizes as well as predictable and reproducible structures and mechanical properties. However, Cu foams with different strengths may be used in actual practice, and thus effective reinforcing approaches need to be carried out, and the strengthening efficiency and mechanisms require carefully evaluated and analyzed.

The mechanical properties of foams closely relate to its density or relative density. In order to compare the strength of the as reinforced foams straightforwardly, the yield stress (σ_y) and the specific yield stress (σ_y/ρ) are plotted in Fig. 8a, and the collapse stress ($\overline{\sigma_{pl}^*}$) and the specific collapse stress ($\overline{\sigma_{pl}^*/\rho}$) are charted in Fig. 8b, based on Tables 1 and 2. It can be seen that the variation of the collapse stresses follows similar trend to that of the yield stress. Both the yield stress and the specific yield stress of S2 and S3 are much lower than those of S1, because the former two samples have lower densities. The yield stress and specific yield stress of S4 are significantly improved compared with S1, and the yield stress and specific stress of S5 are much higher than that of S4. This reflects that compression of a dense Cu pillar or 3-Cu pillars is much difficult than compression of the Cu foam. For S4, both the reinforcing Cu pillar and the foam body are characterized by a uniform plastic deformation, which is evidenced by the image sequence of a1, a2, a3 and a4 in Fig. 9. As the Cu pillar is constrained by the foam body, the inhomogeneous loading that can result in globe buckling or folding of the Cu pillar (as seen in Fig. 7a) is

eliminated. Thus, the synergistic reinforcing effect is achieved and is account for the significant rise in the yield or collapse stress of the “composite” foam structure.

For S5, it can be deduced that the 3 reinforcing Cu pillars remain vertical before the compressing load reaches the yield point (see Figs. 5b and 8). As a result, the increase in yield stress is enormous. As the compressive load increases, however, shear deformation of the Cu pillars occurs, as demonstrated by the b3 image in Fig. 9. The shear deformation is responsible for the load drop in the load–displacement curve illustrated in Fig. 5b, because the shear modulus is much lower than the Young’s modulus for the Cu pillars. Possible inhomogeneous stress which may cause the shear deformation of the pillars results in the lateral deformation of the foam body. The reinforcing pillars are too strong for the foam body to prevent the lateral deformation, resulting in the plateau being replaced by a concave in the load–displacement curve for S5. It is therefore recommended that the strength of the reinforcing pillars and the foam body match each other.

Though lower than the strength of S4, the strength and specific strength of S6 and S7 are much higher than those of the S1. Since the strengths of S6 and S7 are comparable, and the specific collapse stress of S6 is even higher than that of S7, it is less effective for strengthening the Cu foam with 3-Cu tubes than with 1-Cu tube. During compression, the single-Cu tube experienced a cyclic elastic deformation–yield deformation process with a diamond-shaped distortion mode, as demonstrated in Fig. 7b. Repeatedly buckling and folding is responsible for the oscillation of the load–displacement curve. However, the oscillation is eliminated when the Cu tube or tubes is incorporated in the foam body, although the buckling of the Cu tube or tubes are still present during compressing, as respectively shown in c3 and d3 in Fig. 9. It is worth pointing out that the plateau strain at the terminal point of the plateau, ϵ_{pl}^{*t} , of the S6 and S7 are

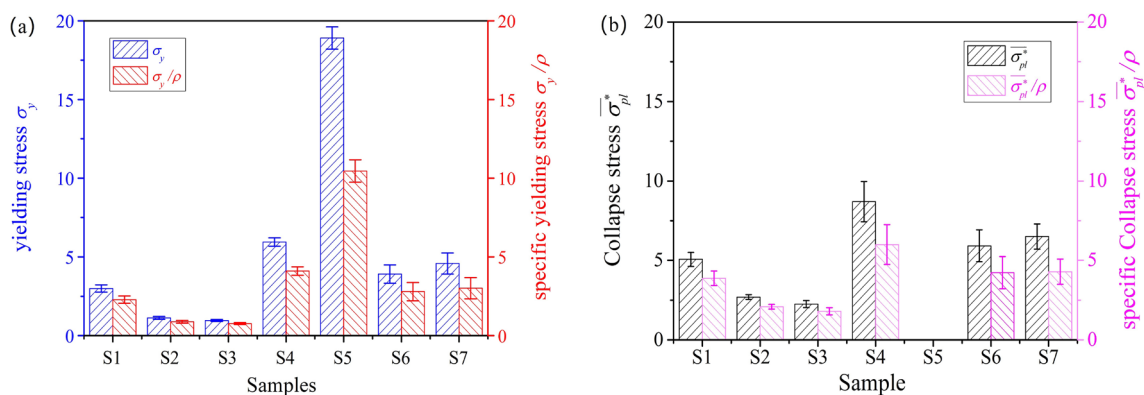


Fig. 8 The yield stress and specific yield stress (a) and the collapse stress and specific collapse (b) of the Cu foam samples

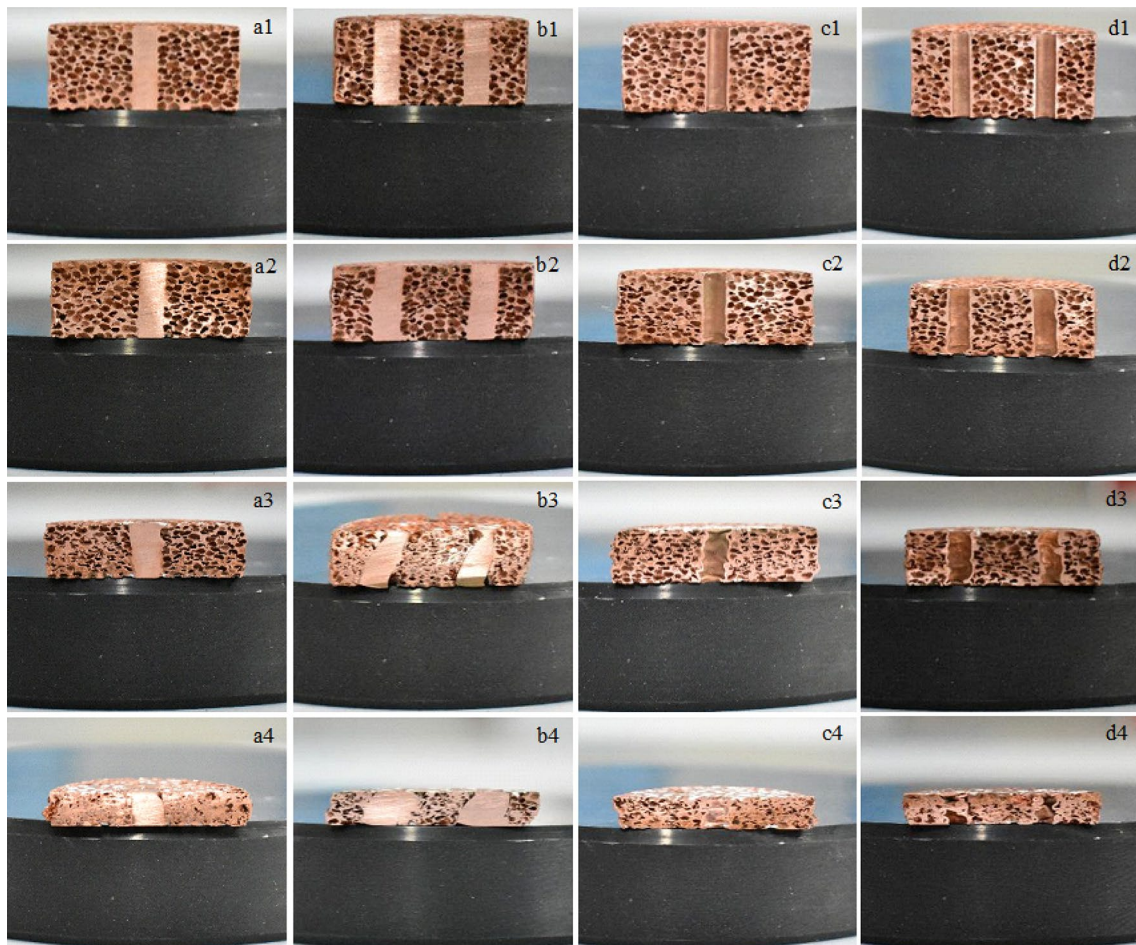


Fig. 9 Deformation morphology of the Cu foam at the middle slicing plane of the Cu pillar(s) or tube(s) parallel to the compression direction at the strain of 0.04 for the first row images, 0.2 for the second-row images, 0.4 for the third row images, and 0.6 for the last row images

greater than that of S1. Higher collapse stress and greater strain will endow S6 and S7 with superior energy absorption compared with the unreinforced Cu foams (S1).

5 Conclusion

In this paper, “composite” copper foams have been successfully constructed by implanting copper pillar(s) or tube(s) into the copper foam body with the aid of positioning device based on a tapping method to interspersing metal powder with a spherical salt bead space holder. The structures and compressive mechanical properties of the “composite” copper foams were studied and the following conclusions were reached:

(1) Implanting copper pillar(s) or tube(s) significantly improves the mechanical properties of the copper foams. The yield strength of S4, S5, S6 and S7 are increased from 3.03 MPa of the foams without reinforc-

ing to 6.84 MPa, 18.91 MPa, 4.24 MPa and 4.75 MPa, respectively.

- (2) The load–displacement curves for the single- or three-copper pillars are similar to that of copper foams. The strength of the single-copper pillar matches that of the copper foam matrix, resulting in optimum properties of “composite” foam structure (i.e. S4). Implanting 3-copper pillars in copper foam matrix causes a strength mismatch between the pillars and the foam matrix. The shear deformation of the 3-copper pillars exerts lateral force on the foam matrix, which exceeds the ability of foam matrix to limit the lateral deformation of copper pillars, resulting in the “composite” foam structure (i.e. S5) losing deformation characteristics of a typical copper foam.
- (3) The load–displacement curves of the single- or three-copper tubes are characterized with a plateau region marked by several rises and falls. Although the strength of the single- or three-copper tubes are much lower than that of the copper foam matrix, the “composite”

structures (S6 and S7) show improved strength and elongated plateau regions of the compression curves. So, the energy absorption capacity of the “composite” structures (S6 and S7) is also increased.

Acknowledgements This work was financially supported by the National Natural Science Foundation of China (no.51461029).

References

- W. Li, H. Jia, C. Pu, X. Liu, J. Xie, Cell wall buckling mediated energy absorption in lotus-type porous copper. *J. Mater. Sci. Technol.* **96**, 82–94 (2015)
- M. Vesenjak, K. Hokamoto, M. Sakamoto, T. Nishi, L. Krstulović-Opara, Z. Ren, Mechanical and microstructural analysis of unidirectional porous (UniPore) copper. *Mater. Des.* **90**, 867–880 (2016)
- M.F. Ashby, R.F. Mehl Medalist, The mechanical properties of cellular solids. *Metall. Mater. Trans. A* **14A**, 1755–1769 (1983)
- P. Lhuissier, Structural properties of solid foams. *C. R. Phys.* **15**, 696–704 (2014)
- C. Kılıçaslan, Numerical crushing analysis of aluminum foam-filled corrugated single- and double-circular tubes subjected to axial impact loading. *Thin Wall Struct.* **96**, 82–94 (2015)
- M.F. Ashby, T. Lu, Metal foams: a survey. *Sci. China Ser. B* **46**, 521–532 (2003)
- A.M. Parvanian, M. Panjepour, Mechanical behavior improvement of open-pore copper foams synthesized through space holder technique. *Mater. Des.* **49**, 834–841 (2013)
- L.P. Zhang, Y.Y. Zhao, Fabrication of high melting-point porous metals by lost carbonate sintering porous process via decomposition route. *Proc. Inst. Mech. Eng. B* **222**, 267–271 (2008)
- N. Bekoz, E. Oktay, Mechanical properties of low alloy steel foams: dependency on porosity and pore size. *Mater. Sci. Eng. A* **576**, 82–90 (2013)
- S.W. Kim, H.D. Jung, M.H. Kang, H.E. Kim, Y.H. Koh, Y. Estrin, Fabrication of porous titanium scaffold with controlled porous structure and net-shape using magnesium as spacer. *Mater. Sci. Eng. C* **33**, 2808–2815 (2013)
- A. Jinnapat, A.R. Kennedy, The manufacture of spherical salt beads and their use as dissolvable templates for the production of cellular solids via a powder metallurgy route. *J. Alloys Compd.* **499**, 43–47 (2010)
- B. Lee, T. Lee, Y. Lee, D.J. Lee, J. Jeong, J. Yuh, S.H. Oh, H.S. Kim, C.S. Lee, Space-holder effect on designing pore structure and determining mechanical properties in porous titanium. *Mater. Des.* **57**, 712–718 (2014)
- D.P. Mondal, M. Patel, S. Das, A.K. Jha, H. Jain, G. Gupta, S.B. Arya, Titanium foam with coarser cell size and wide range of porosity using different types of evaporative space holders through powder metallurgy route. *Mater. Des.* **63**, 89–99 (2014)
- D.C. Dunand, Processing of titanium foams. *Adv. Eng. Mater.* **6**, 369–376 (2004)
- J. Jia, A.R. Siddiq, A.R. Kennedy, Porous titanium manufactured by a novel powder tapping method using spherical salt bead space holders: characterisation and mechanical properties. *J. Mech. Behav. Biomed.* **48**, 229–240 (2015)
- M. Sabzevari, S.A. Sajjadi, A. Moloodi, Physical and mechanical properties of porous copper nanocomposite produced by powder metallurgy. *Adv. Powder Technol.* **27**, 105–111 (2016)
- M. Sharma, O.P. Modi, P. Kumar, Experimental modelling of copper foams processed through powder metallurgy route using a compressible space holder material. *J. Porous Mater.* **24**, 1581–1593 (2017)
- M.H. Shahzeydi, A.M. Parvanian, M. Panjepour, The distribution and mechanism of pore formation in copper foams fabricated by Lost Carbonate Sintering method. *Mater. Charact.* **111**, 21–30 (2016)
- C. Waters, M. Salih, S. Ajinola, Porosity comparative analysis of porous copper and OOF Modelling. *J. Porous Mater.* **22**, 989–995 (2015)
- J. Ru, B. Kong, Y. Liu, X. Wang, T. Fan, D. Zhang, Microstructure and sound absorption of porous copper prepared by resin curing and foaming method. *Mater. Lett.* **139**, 318–321 (2015)
- M. Li, Y. Su, J. Hu, H. Geng, H. Wei, Z. Yang, Y. Zhang, Hydrothermal synthesis of porous copper microspheres towards efficient 4-nitrophenol reduction. *Mater. Res. Bull.* **83**, 329–335 (2016)
- H. Nakajima, S.K. Hyun, K. Ohashi, K. Ota, K. Murakami, Fabrication of copper by unidirectional solidification under hydrogen and its properties. *Colloid Surf. A* **179**, 209–214 (2001)
- H. Seki, M. Tane, M. Otsuka, H. Nakajima, Effects of pore morphology on fatigue and fracture surface of lotus-type porous copper. *J. Mater. Res.* **22**, 1331–1338 (2007)
- S.K. Hyun, K. Murakami, H. Nakajima, Anisotropic mechanical properties of porous copper fabricated by unidirectional solidification. *Mater. Sci. Eng. A* **299**, 241–248 (2001)
- Z. Tang, D. Li, Quasi-static axial buckling behavior of NiTi thin-walled cylindrical shells. *Thin Wall Struct.* **51**, 130–138 (2012)
- R. Sliž, M.Y. Chang, Reliable and accurate prediction of the experimental buckling of thin-walled cylindrical shell under an axial load. *Thin Wall Struct.* **49**, 409–421 (2011)
- X. Luo, J. Xu, J. Zhu, Y. Gao, L. Nie, W. Li, A new method to investigate the energy absorption characteristics of thin-walled metal circular tube using finite element analysis. *Thin Wall Struct.* **95**, 24–30 (2015)
- D. Karagiozova, N. Jones, Dynamic effects on buckling and energy absorption of cylindrical shells under axial impact. *Thin Wall Struct.* **39**, 583–610 (2001)

Publisher's Note Springer Nature remains neutral with regard to jurisdictional claims in published maps and institutional affiliations.